Analysis and correction of track overlapping on nuclear track detectors (SSNTD)

D. Palacios[a], L. Sajo-Bohus[a], H. Barros[a], E. Fusella[b], and Y. Avila[a]
[a] *Universidad Simón Bolívar,*
P.O. 89000, Caracas, Venezuela.
[b] *Instituto de Estudios Avanzados (IDEA),*
Caracas, Venezuela.

Recibido el 10 de marzo de 2010; aceptado el 31 de agosto de 2010

The problem of nuclear track overlapping is addressed assuming the stochastic character of charged particle registry and the fact that even monoenergetic beam perpendicularly impacting on detector surface will show a distribution for track radius values. Asymmetric distributions of overlapping tracks were obtained for very low or very high simulated track quantities, while for intermediate values the distributions were well described by Gaussians. A model for the track overlapping process was developed, considering the dependence of the quantity of non overlapping tracks on the number of simulated tracks by a second order homogeneous differential lineal equation. Its solution contains only one free parameter that is related to track geometry and field view area. By successive approximations, the number of total induced tracks (which is proportional to particle fluence) is determined from the knowledge of the amount of non overlapping tracks, dimensions of the field view and average track radius.

Keywords: Track overlapping; nuclear track detector; Monte Carlo simulation

El problema del solapamiento de trazas nucleares se analiza teniendo en cuenta el carácter estocástico del registro de partículas cargadas y el hecho de que incluso un haz monoenergético, incidiendo perpendicularmente sobre la superficie del detector, mostrará una distribución en los valores del radio de las trazas. Para muy bajas o muy altas cantidades de trazas simuladas se obtuvieron distribuciones asimétricas de trazas no solapadas, mientras que para valores intermedios las distribuciones fueron bien descritas por Gaussianas. Se desarrolló un modelo para describir el proceso de solapamiento de trazas, considerando que la dependencia de trazas no solapadas con el número de trazas simuladas se describe por una ecuación diferencial lineal y homogénea de segundo orden. Su solución contiene sólo un parámetro libre que esté relacionado con la geometría de pista y campo área de visualización. El número total de trazas inducidas (que es proporcional a la fluencia de partículas) se determina por aproximaciones sucesivas a partir del conocimiento de la cantidad de trazas no solapadas, dimensiones del campo de visión y radio medio de las trazas.

Descriptores: Solapamiento de trazas; detector de trazas nucleares; simulación de Monte Carlo

PACS: 29.40.Wk; 29.85.Fj; 02.60.Ed

1. Introduction

Track detectors (SSNTD) are useful devices to qualify and quantify the fluence of charged particles [1]. For low incident particle beam, the registered etched track density is proportional to the fluence, indicating that yield estimates are obtainable in a practical and inexpensive way [2]. In this case, the greatest effect on the total error of yield estimates has a Poisson distribution (random error). There is an upper limit on yield for this method where track overlap starts to be significant [3]. For high fluencies the greatest contribution to the total error is the effect of track overlapping (systematic error). Furthermore, mean track diameters and its dispersion increase at longer etching times so that the quantity of overlapped tracks increases, leading to saturation. For high track density, the probability of underestimating the actual value of track density increases with the use of a semiautomatic system compared with a naked eye, nevertheless in both cases the quantity of non overlapped tracks can be determined with sufficient accuracy. Despite the fact that track overlapping can be a problem in linking track density with particle fluence, few studies on this subject have been carried out, among them we can mention the developed by Yamauchi (2003) [4].

For track count and analysis commercial and homemade programs have been developed. When two or more tracks overlap some software programs count the entire cluster as a unique track while others include specific algorithms to count them properly [5]. Improvements in processing digitalized image of etched tracks and correction for track overlap may significantly extend the upper limit to apply SSNTD for higher yields, overcoming partially at least the limitation inherent to this method. Automated readouts for track density measurements have been developed so to provide better resolution and accuracy even when overlapping tracks exist [6,7]. The track overlap limitation can be extended to considerably higher track densities using also statistical analysis techniques.

When the particle characteristics that hit the detector surface (charge, mass, energy), and its fluence, are unknown, it is very difficult a priori to estimate the exposure times and etching conditions without the risk of obtaining significant track overlap that could affect yield estimates. Due to the varied and complex shapes of overlapped tracks, it is very difficult to determine their quantity. Nevertheless, since most of the digital image analyzers allow to classify tracks by their size and shape [8], more easily if they have simple shapes as quasicirculars, it would be advantageous to develop a method

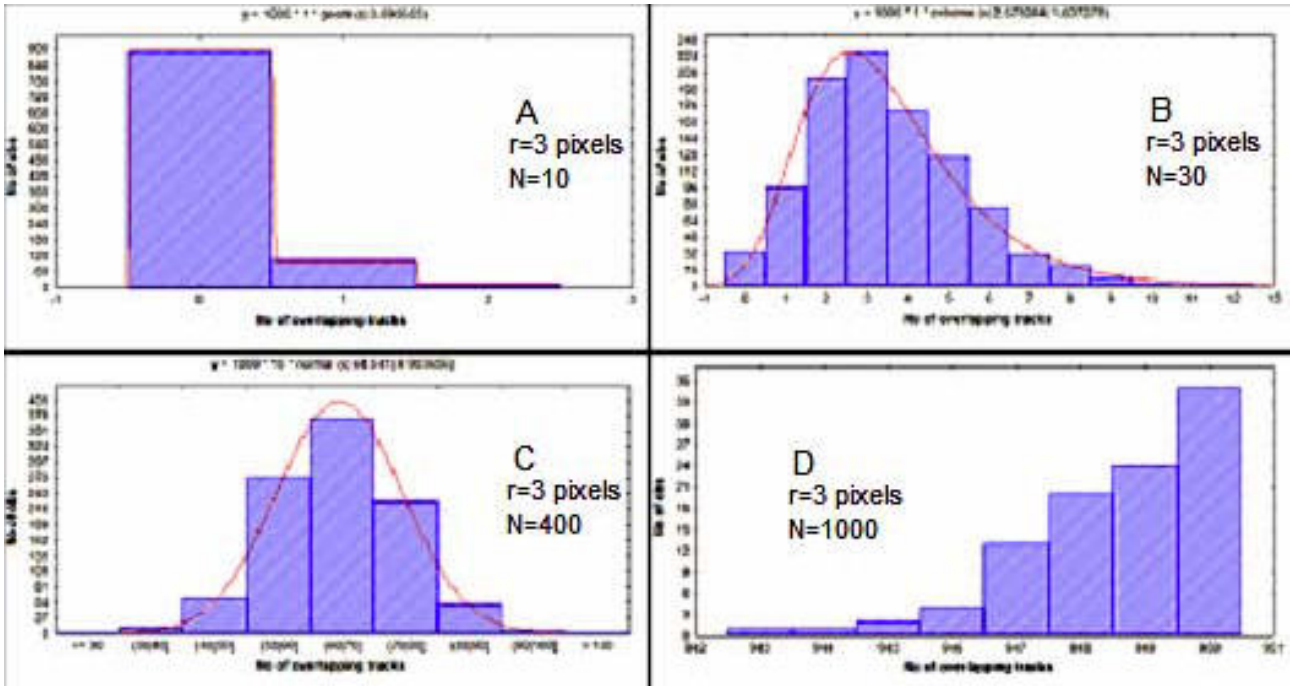

FIGURE 1. Overlapped track distributions (N_s) for different quantities of simulated tracks (N). In all cases the field view was 500×500 pixels^2.

to determine the total amount of tracks induced on a detector from the knowledge of the quantity of non-overlapped tracks. So, the particle fluence or activity could be estimated regardless the degree of track overlapping. This is precisely the aim of this study, but considering quasicircular tracks and the most common real case where tracks are uniformly distributed on detector surface and track radius histograms can be well fitted by Gaussian distributions with certain standard deviation.

2. Simulation of track images

To study the track overlapping process a program in C++ was developed. By means of the program, quasicircular track images can be simulated so that track radii can be fixed or distributed according to a Gaussian distribution with certain standard deviation. For the second case, a normal random variable generator was incorporated in the program. In both cases uniformity in track distributions on detector surface was achieved by means of a Monte Carlo code. Taking into account the stochastic nature of the overlapping process, for each input set (track number to simulate, N, track average radius and its standard deviation, and dimensions of the field view) we collected thousands of simulated track images and in each one the surface distribution and track overlapping was analyzed. The program determined the number of overlapping tracks, N_s, and the amount of non overlapping tracks, N_{ns} ($N_{ns} = N - N_s$). Non overlapping track distributions were obtained by means of the STATISTICA software and were fitted to different distribution functions.

In principle, imaging methods can be used for the overlapping track analysis so that individual tracks of a conglomerate could be discriminated. However, this methodology fails for exact spatial coincidence of two or more tracks or if the cluster is composed of more than three or four overlapping tracks. Our simulation method using Monte Carlo techniques has not such limitations since each time a track is simulated, developed program compares the distances between its center and the centers of all the others (d_{ij}) with the sum of their radios ($r_i + r_j$). Two or more tracks are considered to be overlapping if $d_{ij} \leq (r_i + r_j)$.

3. Overlapped track distributions

Figure 1 shows the distributions of N_s for different quantities of simulated tracks with identical radii, which could have been generated by monoenergetic particles impacting perpendicularly onto the detector surface. Solid lines represent the theoretical distributions that best describe the histograms. The deviation from normality of all distributions was characterized by the Kolmogorov-Smirnov Test [9] at a significance level of 0.05. Analyzing several generated track images for varying parameters we may observe that the histogram departs from the expected normal distribution and it has a strong asymmetrical dependence on the total number of tracks N. For very low N values ($N \leq 10$), when the probability of track overlapping is very small, geometric distribution better describe the N_s histograms (Fig. 1A). Increasing N, so that track overlap becomes significant, the N_s histograms are better described by extreme distributions (Fig. 1B). The distribution of N_s tends to Gaussian for intermediate N values (Fig. 1C). The departure from the normal

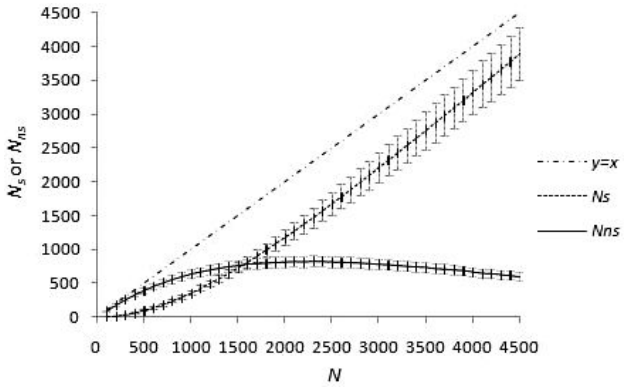

FIGURE 2. Dependence of overlapped (N_s) and non overlapped (N_{ns}) tracks with the total number of simulated tracks (N) for 5 pixels fixed track radii in a 500×500 pixeles^2 field view. Error bars are at 10%.

distribution to the right side (Fig. 1D) is more evident when a large set of tracks are involved ($N >$900).

3.1. Implications of track overlapping distributions

Since track images are generated following a stochastic law, the number of non overlapping tracks corresponding to Fig. 1C is 335±10. It means that if the number of counted tracks (individual) in a the field view is in the range [325,345], then with a 95% probability we can assume that the real number of tracks produced in the detector was 400. This is the track quantity proportional to the particle fluence, which can be determined if the registration efficiency is known. Of course, we have considered that only non overlapping tracks are counted.

4. Etched track overlapping model

Previous study on mathematical etched track modeling suggested that further refinement and improvement were advisable [10]. As further development we introduce the concepts dN_s/dN and dN_{ns}/dN. It is evident that these derivatives shall be directly proportional to the track area (A_T=πr^2) and inversely proportional to the field view area (S).

Typical N_{ns} and N_s dependence with N are shown in Fig. 2. In particular, these results were obtained by simulation of track images of 5 pixels fixed radii in a 500×500 pixeles^2 field view. As shown, few tracks overlap for relatively small N. In this case, N_{ns} is proportional to particle fluence up to approximately 500 tracks, assuming a 10% error, which would represent the critical fluence for that uncertainty level. Track overlapping becomes significant above this critical fluence.

As can be seen in Fig. 2, N_s increases as N gets larger. For relatively small N values the variation of N_s with N significantly increases, but from a certain value (where N_s=N_{ns}) that variation is much smaller. This behavior allows us to assume the concurrence of two processes: increase proportional to N and reduction proportional to N_s. Therefore, the net variation of N_s with respect to N can be assumed proportional to the track number not yet overlapped ($N - N_s$):

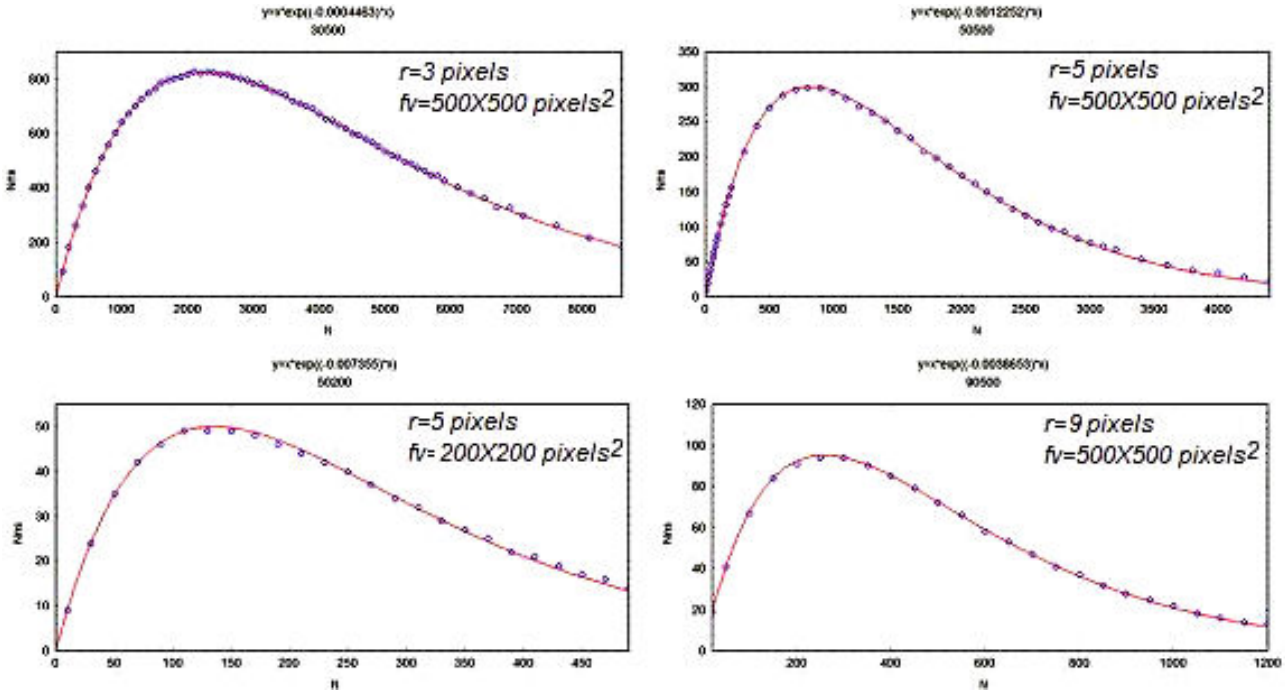

FIGURE 3. Relationship between N_{ns} and N for different track radii and field views.

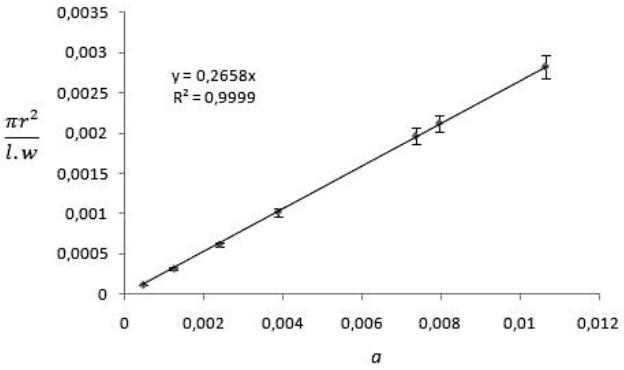

FIGURE 4. Dependence of the quotient between track and field view areas with the a parameters. Error bars are at 5%.

$$\frac{dN_s}{dN} = F\frac{A_T}{S}(N - N_S) \tag{1}$$

As expected, N_{ns} increases as N becomes larger up to a maximum from which gently starts to decrease (Fig. 2). Thus, the slope of the curve is declining to reach zero at the maximum value of N_{ns}, and from there starts to increase but negatively. It can be assumed that the evolution of the number of non overlapping tracks will be set by a dynamic balance, which considers the decrease rate of N_{ns} with respect to N to be proportional to $(N + N_{ns})$:

$$\frac{dN_{ns}}{dN} = -F\frac{A_T}{S}(N + N_{nS}) \tag{2}$$

Proportionality factor F should be the same for both rates due to the interdependence of N_s and N_{ns}. Deriving equation (2) and considering $N = N_s + N_{ns}$, the following expression can be obtained:

$$\frac{d^2N_{ns}}{dN^2} + 2F\frac{A_T}{S}\frac{dN_{ns}}{dN} + \left(F\frac{A_T}{S}\right)^2 N_{ns} = 0 \tag{3}$$

Its general solution is:

$$N_{ns}(N) = (c_1 + c_2N)e^{-aN} \tag{4}$$

where $a = F(A_T/S) = F(\pi r^2/l.w)$, with l and w the length and width of the field view, respectively.

The initial conditions are $N_{ns}(0)$=0 and

$$\left(\frac{dN_{ns}(0)}{dN}\right) = 1,$$

so that the following relationship applies:

$$N_{ns} = Ne^{-aN} \tag{5}$$

From Eq. (5) the N value for which N_{ns} is maximum is $1/a$, so that $N_{ns}^{\max} = 0,368a^{-1}$. The a parameter can be calculated from non-linear fitting of the data to Eq. (5), using the N_{ns} average values obtained by simulation of track images with different track radii and sizes of field views.

5. Validation of the developed method

Figure 3 shows the dependencies of N_{ns} with the total number of simulated tracks using different fixed track radii (r) and field view sizes (*fv*). The solid lines represent the best data fit to Eq. (5).

The results presented in Fig. 3 show that all the N_{ns} vs. N dependencies are well described by the equation obtained according to the developed model. The mentioned characteristic dependence of N_{ns} on N is maintained for different field views and track radii, so that the graph points, defined by the relationship ($\pi r^2/l.w$) *vs.* a, should be well described by a straight line. Figure 4 shows the dependence of ($\pi r^2/l.w$) with the obtained a values. As can be seen, the data are well fitted to a straight line for different track radii and field view areas. The F factor (F=3.7622) was obtained from the slope of the line.

Once the average radius of etched tracks is experimentally determined then the parameter a can be calculated (=$F(\pi r^2/l.w)$) so that the functional dependence between

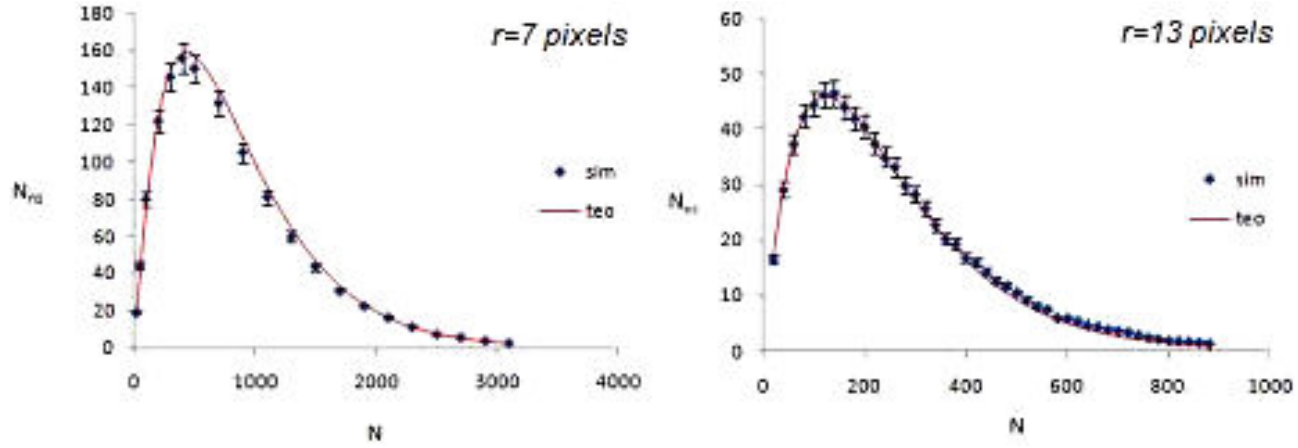

FIGURE 5. Comparison of N_{ns} *vs.* N dependences for results obtained with simulated track images and the predicted by Ec. (5) (solid lines) using the calculated F factor. Error bars represent 5% uncertainty.

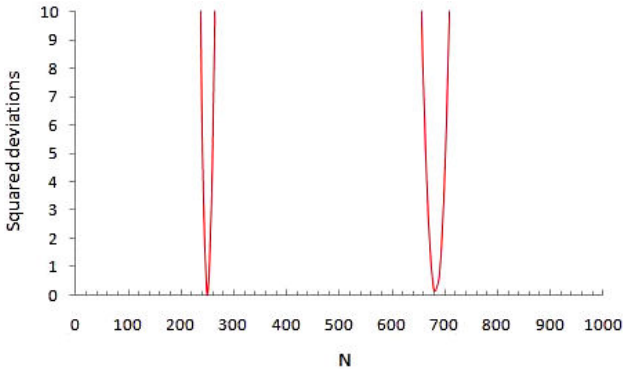

FIGURE 6. Method of successive approximations to calculate the N value that minimizes the squared deviations $\left(Ne^{-aN} - 140\right)^2$.

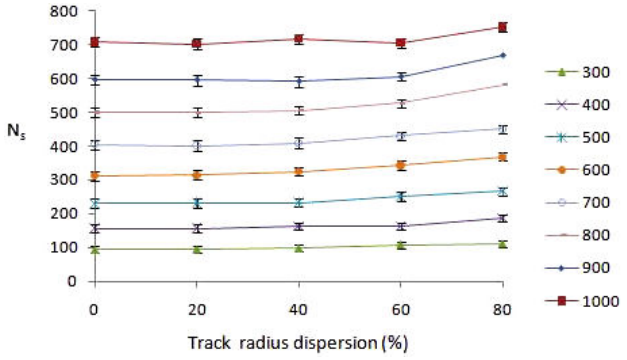

FIGURE 7. Dependence of N_s with the degree of track radius scattering expressed as percentage relative error (%) of average radius. Error bars are at 1σ.

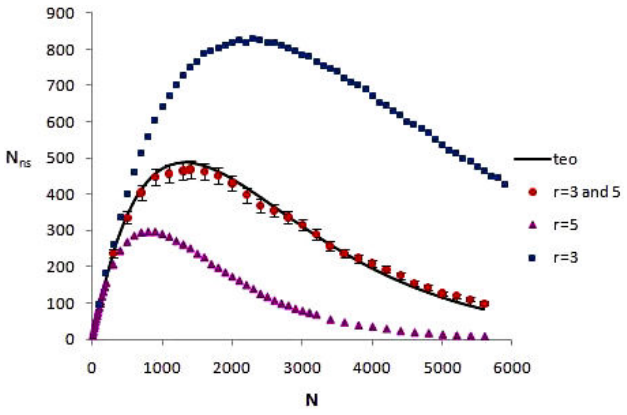

FIGURE 8. Dependences of N_{ns} *vs.* N for track images with fixed radius (3 and 5 pixels) and with radii that randomly can take the value of 3 or 5 pixels. Solid line represents the results obtained from Eq. (5) using the calculated F factor and the average radius (r = 4 pixels).

N_{ns} and N can be known using Eq. (5). As an illustration, Fig. 5 shows the comparisons between the results obtained from the simulated track images and the obtained by Eq. (5) employing only the unique free parameter a determined from the calculated F factor for different track pit areas and 500×500 pixels^2 field view size.

5.1. Example of practical application

Suppose that tracks observed in a 500×500 pixels^2 field view have an average radius of 7 pixels. Using the calculated F factor we obtain a=0,00227, which differs only in 1,28% from the value obtained by the fit of simulation results. If N_{ns} can be determined ocularly or by means of a program, the N value in Eq. (5) (proportional to the particle fluence) can be calculated by a procedure of successive approximations. Suppose also that 140 non overlapped tracks were counted in the field view. By successive approximations two local minima at N=250 and N=680 are found (Fig. 6). These two N values condition the same quantity of non overlapped tracks, with the difference that the first one is before the maximum N_{ns} value (obtained at $N = a^{-1}$= 432) and the second one is after this maximum. By inspection or estimation is easy to recognize the value with physical sense. If N_s is less or the order of N_{ns} then the first value is the correct, but if $N_s \gg N_{ns}$ the right value is the second one (see Fig. 2).

6. Overlapping for dispersed track radii

So far we have deal only with fixed track radii but experimentally track radius distributions with some standard deviation about the mean are commonly observed [11,12]. To evaluate the effect of track radius distribution on the overlapping process, track images with Gaussian radius distribution were simulated. Different track quantities in a 500×500 pixels^2 field view, with 5 pixels mean track radius and standard deviation ranging from 0 to 80% about the mean were simulated. Figure 7 shows that N_s does not significantly depend on the degree of track radius dispersion for any quantity of simulated tracks. This result is very important since results obtained for fixed radii are also applicable if track radii have some distribution with relative error not exceeding 60%. Thus, the developed model can be applied with strength for the case of particle beams even if they have relatively large scattering either in energy or mass.

For a given number of simulated tracks, at least up to 60% the increase of track radius dispersion produces no significant variation both in the average number of overlapping tracks and its scattering

7. Overlapping for aleatorly mixed track distributions with different average radii

Commonly, distributions of two or more groups of tracks differentiated by their average radius may appear (for example, when particles with different average energy impact the detector surface). As an illustration, Fig. 8 shows the dependences of N_{ns} with N for the case of tracks with the same radius and when both types of tracks are randomly (uniformly) distributed in the field view.

As can be seen, Eq. (5) also properly describes the relationship between N_{ns} and N, with an error of less than 5%,

when the average radius is used to characterize track images with two sets of tracks with well defined radii. However, when the difference between track radii is relatively large (*e.g.*, 3 and 15 pixels), the previous procedure fails for large N values, *i.e.* after reached the N_{ns} maximum value. Therefore, for broad energy spectrum particle beams impacting on a detector the interaction of tracks with different radii should be considered. In that case the use of a multi-exponential model can generate satisfactory results.

8. Conclusions

The distribution of non overlapping tracks depart from normality and an interval of values exists for N values where the normal distribution is satisfied being this a limitation for some applications.

A method to determine particle beam intensity from etched track density simulation is given. A simple model, with a single free parameter, that relates the number of non overlapping tracks with the total was developed for quasi-circular tracks. The model adequately describes the dependences for a wide range of track radii and dimensions of the field view.

One of the most interesting results is that the total number of tracks produced in a detector, which is proportional to the particle fluence, can be predicted if the quantity of non overlapping tracks is experimentally determined, offering an improvement for track density interpretation in complex calibration studies.

The developed model is also applicable for Gaussian track radius distribution, which is the case of particle beams with scattering either in energy or mass. The average number of overlapping tracks and its dispersion do not significantly change even for relatively large dispersions of track radius.

The main advantage of the developed method is related with the possibility to determine the impinging particle fluence independently of the overlapping degree since only quasicircular tracks are analyzed. The track overlap limitation can be extended to considerably higher track densities.

1. J. Palfalvi, L. Sajo-Bohus, and I. Eordogh, *Rad. Meas.* **31** (1999) 157.
2. T. Yamauchi, *Rad. Meas.* **36** (2003) 73.
3. D. Palacios, F. Palacios, L. Sajo-Bohus, and J. Pálfalvi, *Rad. Meas.* **34** (2001) 119.
4. J.A. Frenje *et al.*, *Rev. Sci. Instrum.* **73** (2002) 2597.
5. K. Amgarou *et al.*, *Rad. Meas.* **33** (2001) 203.
6. G. Sciocchetti, G. Cotellessa, S. Tosti, P.G. Baldassini, and E. Soldano, *Proceedings of the Fifth International Symposium on the Natural Radiation Environment* (Salzburg, September, 1991). p. 22.
7. D.L. Patiris, K. Blekas, and K.G. Ioannides, *Nucl. Instrum. Methods Phys. Res., Sect. B* **244** (2006) 392.
8. L. Sajo-Bohus, J. Palfalvi, and E.D. Greaves, *Rad. Phys. Chem.* **51** (1998) 467.
9. D. Palacios and L. Sajo-Bohus, *Proceedings of CIMENIC2004. Simulación Numérica y Modelado Computacional*. J. Rojo, M.J. Torres y M. Carrolaza Editores. (Caracas, 2004 SVMNI. TC-43-50).
10. P.A. Lapitz, J. Ruzzante, and M.G. Alvarez, *Revista Materia* **10** (2005) 370.
11. A.S. Roussetski, *Proceedings of the 8th International Conference on Cold Fusion* (Lerici (La Spezia), Italy: Italian Physical Society, Bologna, Italy, 2000).
12. M.F. Zaki and Y.H. El-Shaer, *PRAMANA - Journal of Physics* **69** (2007) 567.